On the Local Relaxation of Solid Neon upon Rydberg Excitation of a NO Impurity: The Role of the NO(A)−Ne Interaction Potential and Zero-Point Quantum Delocalization†

Pedro Pajón-Suárez,‡,§ Germán A. Rojas-Lorenzo,‡ Jesús Rubayo-Soneira,‡ Ramón Hernández-Lamoneda,§ and Pascal Larrégaray*,||

Instituto Superior de Tecnologías y Ciencias Aplicadas, Quinta de los Molinos, Avenida Salvador Allende y Luaces, Plaza C. Habana, Cuba, Centro de Investigaciones Químicas, Universidad Autónoma del Estado de Morelos, Av. Universidad 1001, Cuernavaca, Morelos 62210, Mexico, and Institut des Sciences Moléculaires, Université Bordeaux 1/CNRS, 351 Cours de la Libération, 33405 Talence Cedex, France

Received: April 17, 2009; Revised Manuscript Received: August 6, 2009

The local relaxation of solid neon subsequent to the impulsive excitation of the NO chromophore to its A(3sσ) Ryberg state is investigated using molecular dynamics simulations. This study makes use of empirical NO(X,A)−Ne isotropic pair potentials as well as a recently developed *ab initio* triatomic potential energy surface for the excited state. The role of these interaction potentials is analyzed, including many-body effects. In particular, empirical potentials, designed to reproduce correctly both the NO X−A steady-state absorption and emission bands, are shown to lead to a good description of the subpicosecond relaxation dynamics. The 600 fs expansion of the electronic bubble fairly agrees with experimental data. This relatively long time scale with respect to solid Argon, which was previously attributed to the range of the NO(A)−Ne interaction, is presumably related to the quantum nature of the medium. The time-resolved local relaxation of the Ne solid is understandably intermediate between that of classical solids (e.g., Ar) and that of quantum solids (e.g., H_2).

1. Introduction

The investigation of extensive configurational rearrangements following photoabsorption of many body systems is of primary interest in condensed-matter physical chemistry and biology.[1] In connection with experiments, molecular dynamics (MD) computer simulations have proven to be a valuable tool to get insight, at the molecular scale, into such processes originated in liquids,[2−7] solids,[4,8−17] and clusters,[9,10,18−20] which usually involve intra- and intermolecular motions inducing long-range propagation of energy into the medium.

To rationalize the photoinduced configurational rearrangements, pure and doped rare-gas media might serve as model systems[21,22] because of their well-known physical and thermodynamical properties associated with their simple structures. Among model systems, solid neon has been experimentally scrutinized via electronic absorption/fluorescence spectroscopy[1,21−27] and more recently via femtosecond pump−probe spectroscopy.[28] In the latter experiments, the dynamics of the electronic bubble, created through an ultrafast transition to the spatially extended A(3sσ) Ryberg state of a NO chromophore, is followed in real time. Because of the non-negligible zero-point amplitude motions, solid neon is a particularly interesting model to investigate the influence of quantum effects on energy dissipation mechanisms. Such quantum effects, which do not take place in so-called classical solids,[29−33] strongly influence steady-state spectroscopy[34,35] and significantly affect the dynamics of structural relaxation.[36−39] In particular, the subpicosecond coherent local relaxation of classical solids mediated by localized modes does not appear in solid hydrogen, where energy tends to dissipate irreversibly into the medium over such a time scale.[37−39]

The theoretical description of the structural dynamics following the photochemical excitation of chromophores embedded in rare-gas solids[40−46] and molecular hydrogen[37−39] has been achieved in the last years. The structural relaxation upon impulsive Rydberg excitation of NO-doped solid neon has been recently investigated using nonequilibrium classical molecular dynamics (MD) simulations[43,44,46] in which the quantum zero-point motions of the lattice atoms have been approximately accounted for.[47] In these previous works, the NO molecule was considered to be an atom so that the NO(X)$^2\Pi$−Ne and NO(A)$^2\Sigma$−Ne intermolecular interactions were approximated by isotropic pair potentials. The angular anisotropy, which is substantial in the excited state (about 8% of the isotropic part[50]), was neglected on the grounds that: (i) the effects induced by the electronic excitation are by far more dramatic and (ii) the significant amplitude zero-point motion of Ne atoms about the lattice sites is expected to average out anisotropic contributions.[49] This approach[31,32] reproduced the main characteristics of the solid dynamical relaxation upon photoexcitation. The relative slower electronic bubble expansion in Neon (∼600 fs),[28−43] as compared with that in Ar (∼250 fs),[41] was attributed to the larger range of the repulsive part of the interaction in NO (A)−Ne. In argon, the first shell surrounding the NO chromophore (12 atoms) impulsively moves outward upon excitation, whereas three neighboring shells are instantaneously set in motion in neon (42 atoms). The contribution of the zero-point quantum effects was found to be negligible.

Very recently, similar experimental and theoretical studies in *para*-hydrogen revealed an even slower bubble expansion time scale (∼800 fs) despite a much lighter mass for the medium atoms.[37−39] It was observed that the first shell expands freely over 50−100 fs and then merges into the second and third shells,

† Part of the "Vincenzo Aquilanti Festschrift".

* Corresponding author. E-mail: p.larregaray@ism.u-bordeaux1.fr.
‡ Instituto Superior de Tecnologías y Ciencias Aplicadas.
§ Universidad Autónoma del Estado de Morelos.
|| Université Bordeaux 1/CNRS.

10.1021/jp903538f
Published on Web 09/15/2009

slowing down the expansion to 800 fs. This effect is strongly related to the local disorder of solid hydrogen due to the zero-point quantum delocalization of the host matrix molecules.

These last results in *para*-hydrogen along with the insufficient agreement of the computed steady-state and time-resolved spectroscopy features in our previous work led us to reconsider the problem. To that end, some of us recently developed a new potential energy surface (PES) for the first Rydberg excited state of Ne−NO complex using high-level ab initio quantum chemistry techniques.[50] The main motivation of the present work is to evaluate whether the inclusion of the details of the NO−Ne interaction, namely, its angular dependence, into the simulation of the Ne structural relaxation leads to a better agreement with experimental results and thus improves our understanding. The outline of the article is the following: In Section 2, we present the theoretical methodology associated with the intermolecular potentials used and MD procedure in our simulations. In Section 3, we present the results and discussion. Finally, some conclusions are drawn in Section 4.

2. Methodology

2.1. Intermolecular Potentials. The Ne−Ne interaction is modeled by a Morse potential

$$V_{ij} = D_0[1 - e^{-\beta(r_{ij}-r_e)}]^2 - D_0 \quad (1)$$

where D_0, β, and r_e are the Morse parameters taken from ref 51 and $r_{ij} = |\mathbf{r}_j - \mathbf{r}_i|$ is the interatomic distance between i and j neon atoms. This potential, which was developed to study the vibrational predissociation of van der Waals clusters,[51] is in good agreement with the best estimates to date.[52]

The steady-state spectroscopy as well as the dynamics of the NO impurity embedded in solid neon has been investigated using different intermolecular interaction potentials, depending on the NO electronic state. The NO(X)−Ne ground-state interaction potential has been approximated with a Lennard-Jones potential taken from a previous study.[43]

Three different interaction potentials for the NO(A)−Ne excited state have been developed. The first one was generated by fitting the fluorescence−excitation spectra of the NO−Ne complex in the region of the A-state absorption measured by Levy et al.[53] The interaction is considered to be isotropic because the Rydberg electron is in a nearly spherical orbital and, as already discussed in ref 41, the excited-state intermolecular potential is most likely purely repulsive. As we will show later, this approximation is not entirely justified as the ab initio calculations indicate significant anisotropy in the Franck−Condon region. This potential is approximated by a Born−Mayer (BM) function[43,54]

$$V(r) = A \exp\left[-\left(\frac{r - r_0}{b}\right)\right] \quad (2)$$

where A, r_0, and b are the BM parameters. It is important to notice that the NO(A)−Ne potential was fitted to reproduce experimental data for the Ne−NO complex in a small energetic window around the absorption band (repulsive arm of the excited potential−short-range part of the potential). This potential is referred as the BM potential in the following. To improve the agreement between the experimental and calculated absorption line shapes for NO embedded in the Ne solid, a different BM potential for the NO(A)−Ne interaction was proposed.[43] This potential is referred to as the adjusted BM potential in the following.

TABLE 1: Parameters of the Potentials Used for: (a) Ne−Ne Potential, (b) NO(A)−Ne Adjusted Morse Potential, (c) NO(A)−Ne BM Potential, and (d) NO(A)−Ne Adjusted BM Potential

	D_0 (cm^{-1})	β (Å^{-1})	r_e (Å)
Ne−Ne (a)	29.36	2.088	3.091
NO(A)$^2\Sigma^+$−Ne (b)	4.0325	0.96	6.0
	A (cm^{-1})	r_0 (Å)	b (Å)
NO(A)$^2\Sigma^+$−Ne (c)	2000.0	2.6	0.6
NO(A)$^2\Sigma^+$−Ne (d)	2114.986	2.182	0.752

In addition, in previous time-resolved studies on the dynamics of photoinduced structural rearrangements in quantum solids[37−39] and supercritical fluids,[55] empirical pair potentials for the NO(A)−H_2 and NO(A)−Ar interactions were proposed. Both potentials, which were developed to reproduce correctly the NO A−X absorption and emission bands via equilibrium MD simulations, present shallow wells at medium range. Such potentials were subsequently used in nonequilibrium MD simulations to predict the structural reorganization following an impulsive excitation of the NO chromophore, leading to a satisfactory agreement with pump−probe femtosecond experiment.[37−39] Following these lines, we developed a Morse pair potential (eq 1) for the NO(A)−Ne interaction bearing a shallow well around 6 Å. The steady-state spectroscopy features are properly reproduced by MD simulations using this potential. (See the next section for details.) This potential is referred to as the adjusted Morse potential in the following.

The parameters of all of these fitted potential are given in Table 1.

Besides the development of the empirical pair potential presented above, the NO(A)−Ne PES has been calculated using highly accurate ab initio calculations.[50] In these calculations, the Jacobi coordinate system ($\mathbf{r}_{NO}$, r, α) was used, where r is the intermolecular distance of Ne atom from the center of mass of NO, $\mathbf{r}_{NO}$ is the NO bond length, and α is the angle between the r and $\mathbf{r}_{NO}$ vectors. A grid of intermolecular energies (r, α = 0, 45, 90, 135, and 180°) was computed, restricting the NO bond length at its equilibrium position. To perform the MD simulation, the ab initio points were fitted by cubic splines for each Jacobi angle, and collocation methods were used to explore all directions around the center of mass of NO. Global analytical representation of the PES was derived. Details can be found elsewhere.[50]

2.2. Molecular Dynamics. The details of the classical equilibrium and nonequilibrium MD simulations, which are based on a standard procedure,[56] have already been given in previous works.[37−39,41−45,55] To mimic the quantum effects in classical MD, the so-called quantum harmonic temperature correction proposed by Bergsma et al.[47] was used. This correction, which was recently discussed in detail,[47,59] including its effect on the relaxation dynamics, allows us to describe with a reasonable accuracy the local structure and the steady-state spectroscopic data (Stokes shifts, lineshapes, etc.) for quantum solids[37,38] without increasing the computational effort. A temperature of 37 K is used in our simulations. As a comparison, the energy transferred to the matrix upon electronic excitation corresponds to 580.6 K/atom when equally shared over the 18 atoms constituting the first two shells. As previously suggested,[37,38] at short times, the quantum nature of the environment is

anticipated to play a role exclusively through the spatial delocalization of the lattice atoms, which is approximately accounted for by the quantum harmonic temperature correction.

The temporal evolution of the system was simulated by the numerical integration of the classical equations of motion of 499 or 1371 Ne atoms and 1 NO molecule arranged in an FCC lattice. The NO molecule is supposed to sit in one "main" substitutional site.[60,61] The lattice physical parameters are taken from a previous study.[43]

The system is described by the following Hamilton function

$$H(\mathbf{r},\mathbf{p}) = \sum_{i=1}^{N} \frac{p_i^2}{2m_i} + V(\mathbf{r_1},\mathbf{r_2},...,\mathbf{r}_N) \quad (3)$$

In this formula, $\mathbf{r}$ is the particle position vector and $\mathbf{p}$ its conjugate momentum. When the NO molecule is considered to be a spherical atom, as in previous studies in which the chromophore rotational and vibrational degrees of freedom were not expected to affect the structural relaxation dynamics,[43,37,38] the potential energy is computed to be the sum of the isotropic pair potential presented above

$$V(\mathbf{r_1},\mathbf{r_2},...,\mathbf{r}_N) = \frac{1}{2}\sum_{i=1,i\neq j}^{N}\sum_{j=1}^{N} V_{ij}(r_{ij}) \quad (4)$$

where $V_{ij}(r_{ij})$ represents the different pair interaction potentials.

When the NO(A)−Ne interaction is represented by an ab initio PES, the force acting on the ith atom is computed by finite differences, as shown in the following expressions.

$$\begin{aligned} f_{x_i} &= -[U(\vec{r}_1,\vec{r}_2,...,x_i+\Delta x,...,\vec{r}_N) - \\ &\qquad U(\vec{r}_1,\vec{r}_2,...,\vec{r}_i,...,\vec{r}_N)]/\Delta x \\ f_{y_i} &= -[U(\vec{r}_1,\vec{r}_2,...,y_i+\Delta y,...,\vec{r}_N) - \\ &\qquad U(\vec{r}_1,\vec{r}_2,...,\vec{r}_i,...,\vec{r}_N)]/\Delta y \\ f_{z_i} &= -[U(\vec{r}_1,\vec{r}_2,...,z_i+\Delta z,...,\vec{r}_N) - \\ &\qquad U(\vec{r}_1,\vec{r}_2,...,\vec{r}_i,...,\vec{r}_N)]/\Delta z \end{aligned} \quad (5)$$

As implemented in several previous studies,[41−44,37−39,55] the absorption and emission lineshapes are computed through long equilibrium trajectories considering, respectively, the NO(X)−Ne or the NO(A)−Ne interaction potentials. The real time response of the system is investigated via nonequilibrium MD simulation. Uncorrelated configurations are taken from an equilibrium trajectory for NO in the ground electronic state. The subsequent electronic transition is simulated by switching to the excited-state potential and following the numerical integration of the equations of motion on this PES.

The nuclear motion in response to the excitation of the NO molecule is visualized by the temporal evolution of the radii of up to the tenth coordination shell

$$R_k(t) = \frac{1}{n_k}\sum_{j=1}^{n_k} |\mathbf{r}_j^{n_k}(t) - \mathbf{r}_{NO}(t)| \quad (g)$$

which corresponds to the mean distance between NO($A^2\Sigma^+$) and the kth shell of solid atoms. All trajectories were averaged over 100 individual trajectories of the shell radius. For the FCC lattice, the first shell contains 12 atoms. To get more insight into the simulated medium response, we also computed time-dependent radial distribution functions with two unit cells containing 1 NO molecule with 499 and 1371 Ne atoms, respectively. The way to compute these quantities has been already detailed elsewhere.[37−39]

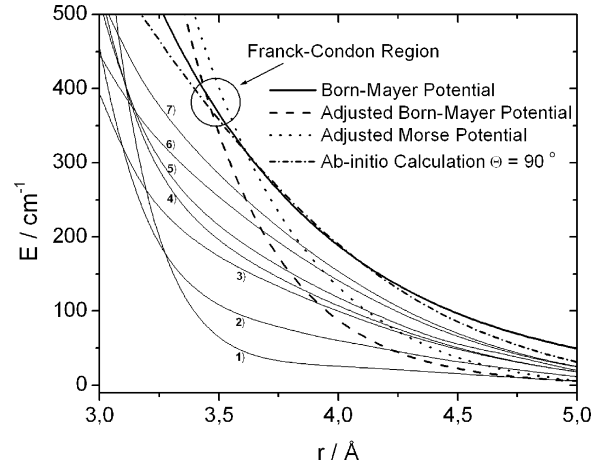

Figure 1. Cuts of the *ab initio* interaction potential as a function of r for several angular configurations and fitted interaction potentials used in this work. The labels correspond to: (1) 0, (2) 30, (3) 45, (4) 180, (5) 160, (6) 60, and (7) 135°.

3. Results and Discussions

In Figure 1, the interaction potentials for the different angular configurations studied at the *ab initio* level and the empirically fitted potentials are shown. In the Franck−Condon region (close to 3.5 Å), the slopes of the adjusted Born−Mayer and Morse potentials are comparable. This similarity is to be expected given that they have been constructed to reproduce both the experimental absorption and emission bands. The slopes of the T-shape ($\alpha = 90°$) cut of the *ab initio* PES and the Born−Mayer-fitted (c in Table 1) potential are also similar. The T-shape geometry corresponds to the equilibrium structure of the NeNO(X) complex. As has been previously discussed, this similarity ascertains the quality of the *ab initio* calculations.[50] All of these potentials are close to each other in the Franck−Condon region. Nevertheless, it has to be noticed that the range of the repulsive part of the adjusted BM and Morse potentials is shorter than the previously used BM potential. It is also worth mentioning that the *ab initio* interaction potential shows a strong angular dependence in the FC region, and in this sense, the reliability of the isotropic empirical potentials is questionable. After excitation, considering the *ab initio* PES, the anisotropic contribution to the average energy per atom in the two first shells is about 24 K, which is only 4% of the excitation energy (580.6 K/atom, as previously mentioned). This energy, which compares with the thermal correction, suggests that anisotropy should not play an important role in relaxation dynamics at short times, as discussed later.

Figure 2a shows the absorption and emission bands simulated using the 1D potential at the T-shape configuration and the 2D PES resulting from ab initio calculations.[50] The steady state spectroscopic bands simulated with the Born−Mayer interaction potential generated by fitting the fluorescence−excitation spectrum of the NeNO complex and the experimental results are also shown. The absorption bands are similar, but the locations of the emission bands are quite different. In particular, the Stokes

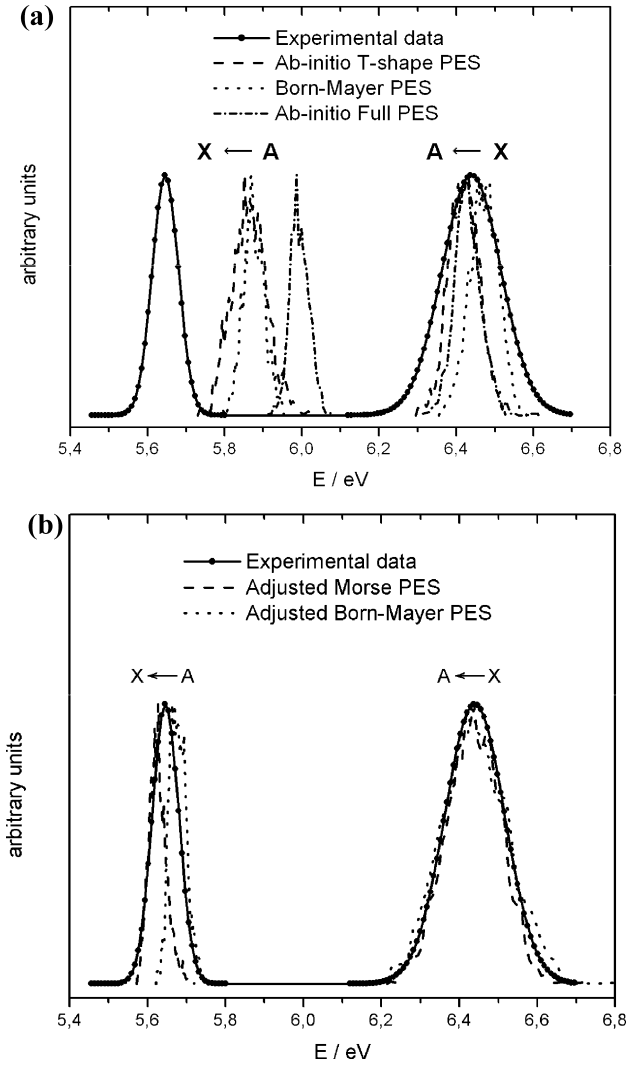

Figure 2. Simulated steady-state spectroscopy considering (a) the T-shape ($\alpha = 90°$) cut of the ab initio PES, the total ab initio PES,[37] the BM potential fitting the PES in the excited state, and the experimental results and (b) the adjusted Morse and BM potentials and the experimental results.

shifts for the Born−Mayer potential and T-shape configuration show analogous behavior and correspond to 75% of the experimental value. The similarity of results for the Born−Mayer potential and the T-shape configuration of the PES is a direct consequence of a similar value in the Franck−Condon region. Using the full PES, we obtain a Stokes shift, which is only 56% of the experimental value. In Figure 2b, the steady-state bands computed using the adjusted BM (d) and Morse potentials are displayed. In both cases, the simulations are able to reproduce the experimental observations properly. The experimental and calculated steady-state spectroscopic bands shown in this work are related to the NO occupying a "main" site in the Ne matrix. Although spectroscopic experimental data about NO occupying a "red" site in the crystal are available, to our knowledge, no simulations have considered this possibility.

In Figure 3, we show the nearly isotropic behavior for the excited state, where two very shallow wells appear, localized close to the O and N atoms. The latter is more localized but does not modify the isotropy of the PES drastically. The anisotropy contribution has been estimated to be the ratio between the sum of the squares of the radial functions appearing in the usual Legendre expansion, excluding and including the isotropic terms. For the excited state, it corresponds to 8.28%.[50]

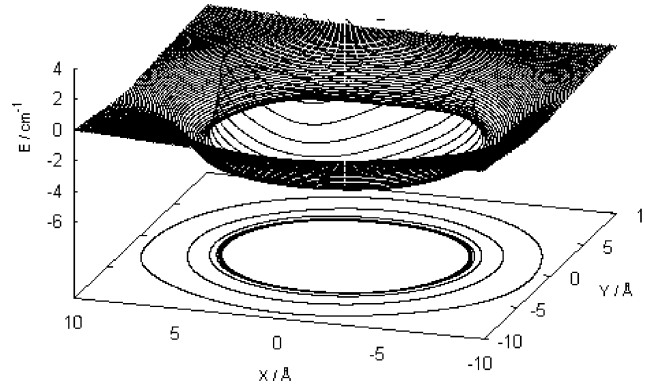

Figure 3. Contour plot of the interaction potential in the Cartesian plane for Ne−NO(A) with the origin at the NO center of mass.

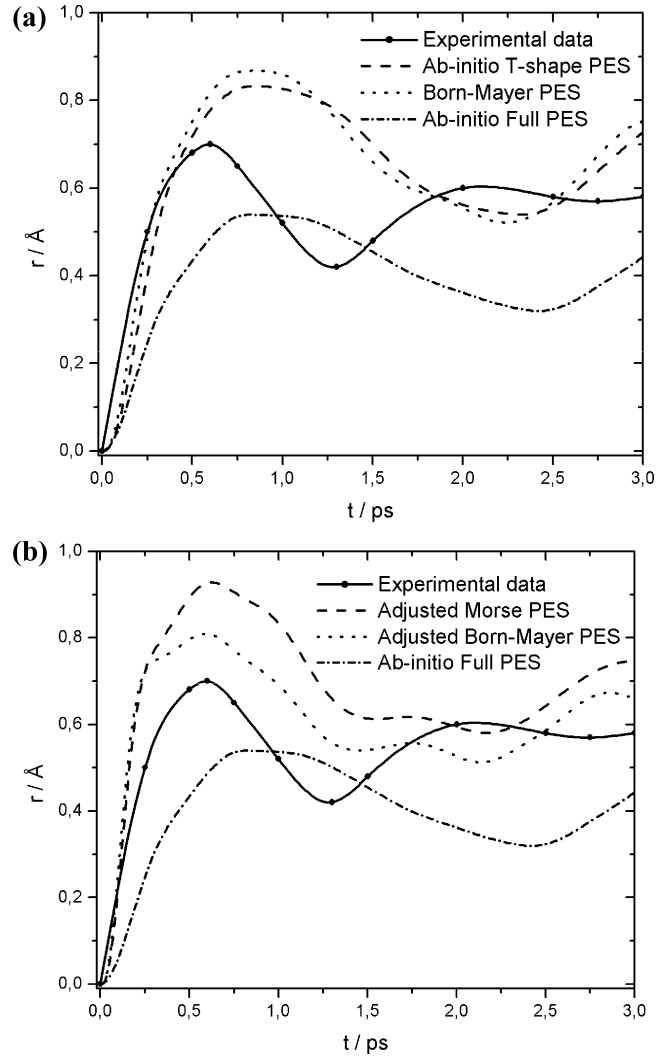

Figure 4. Time dependence of the first shell radius. (a) T-shape ($\alpha = 90°$) configuration of the *ab initio* PES, Born−Mayer fitted potential (c in table 1), *ab initio* full PES, and experimental result. (b) Adjusted Morse and Born−Mayer potentials in comparison with full ab initio potential and experimental data.

It is important to stress that this analysis corresponds to the region of the van der Waals minimum of the complex. As stated above in the repulsive part of the potential, the degree of anisotropy is much larger.

In Figure 4a,b, the time dependence of the average cage radius out of 100 individual trajectories for the first shell around the NO impurity is represented for 500 atoms in the primitive

simulation cell. This shell is defined here as the average position of the 12 nearest Ne atoms (FCC lattice). In both Figures, the simulated dynamical relaxations using the various NO(A) potentials are compared with the pump−probe femtosecond spectroscopy result. The time evolution using the T-shape potential and the Born−Mayer fitted potential (c in Table 1) and the full ab initio PES are very similar (Figure 4a). The first expansion−contraction event occurs by 2.25 to 2.5 ps, delayed with respect to the experimental result (about 1.4 ps). The amplitude of the first expansion, using the full ab initio PES is smaller than the experimental one, whereas those obtained with the T-shape potential and the Born−Mayer fitted potential are larger. Figure 4b shows the dynamical response of the system for the adjusted Born−Mayer and Morse potentials. Although the amplitude of the first expansion event is larger, the first expansion−contraction time scale is in reasonable agreement with the experimental response (by 1.35 to 1.45 ps). The results presented in Figure 4a,b suggest that the details of the $NO(A)^2\Sigma^+$−Ne potential at long-range (i.e., in the attractive part) are not significant for the dynamics on the short time scale by analogy to what was found for $NO(A)^2\Sigma^+$−Ar.[29] The explanation for the observed dynamical response induced by the different potentials can be traced back to their slopes and the potential energies in the FC region, where those that were adjusted to fit experiment have larger values than those based on ab initio calculations or spectroscopy of the NeNO complex. Considering the 1D effective bubble model[21,49] used to interpret the experimental pump/probe signals, the relaxation is given by the time evolution of a nearest neighbors' cage radius. The force acting on the radius is directly related to the slope of the excited-state pair potential. As a consequence, the greater the slope, the faster the expansion−contraction event.[43]

The first expansion−contraction event simulated employing the adjusted Born−Mayer and Morse potentials reveals different amplitudes (Figure 4b). This difference presumably arises from the relative shift of both potentials in the Franck−Condon region (Figure 1), which involves a different energy release into the medium upon excitation. The behavior observed in Figure 4a can be understood in an analogous way. The case of the full ab initio potential deserves special mention. As we can see in Figure 4a, the first expansion amplitude for this case is the smallest and should be related to the cuts of the full PES in several angular configurations. The slopes of these cuts as well as the total energy released in the system (proportional to the absolute value of the interaction potential) are the smallest in the Franck−Condon region.

It has to be noticed that experimentally the time evolution of the bubble radius is inferred from pump/probe signals within the framework of the configuration coordinate model.[21,49] This 1D harmonic interaction model for the NO(X,A)−matrix interaction (42 and 58 cm^{-1} respective frequencies) together with the limited pump/probe cross correlation (fwhm ∼320 fs) intrinsically influence the dynamical experimental response, as mentioned in ref 28.

Figure 5a,b displays the time evolution of the Ne radial distribution function around the NO impurity after the X−A electronic transition. In these simulations, the NO(A)−Ne-adjusted Morse interaction potential was used. Two cubic simulation cells containing (a) 500 and (b) 1372 atoms were used, the sides of which were, respectively, 22.34 and 31.28 Å. In the first case (a), the perturbation caused by the electronic transition reaches the limit of the simulation shell within ∼800 fs, whereas it takes more than 1 ps for the largest simulation cell. Consequently, as shown in Figure 5c, the first-shell

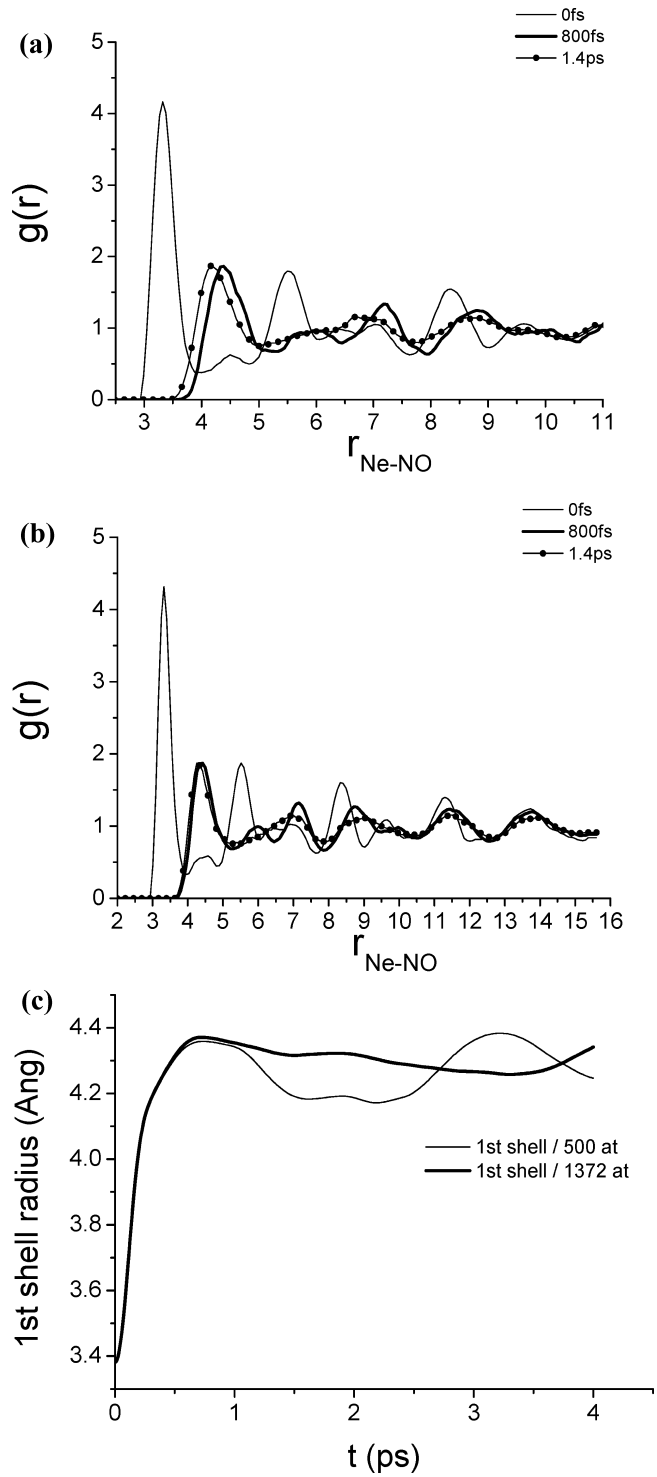

Figure 5. Time-dependent radial distribution functions of Ne around the NO impurity for simulation cells containing (a) 500 and (b) 1372 atoms. (c) Time evolution of the first shell radius defined by eq g for both simulation cells.

simulated dynamical response, as defined by eq g, appreciably depends on the size of the simulation cell on the picosecond time scale. Moreover, within this time scale, the excess energy released by the electronic transition (about 0.9 eV), is spread over the entire simulation cell. When considering a unit cell of 500 atoms, this energy corresponds to approximately 20 K per atom (if equally shared), which is comparable to the thermal quantum correction we employ to account for zero-point energy delocalization. As a consequence, the MD simulations performed

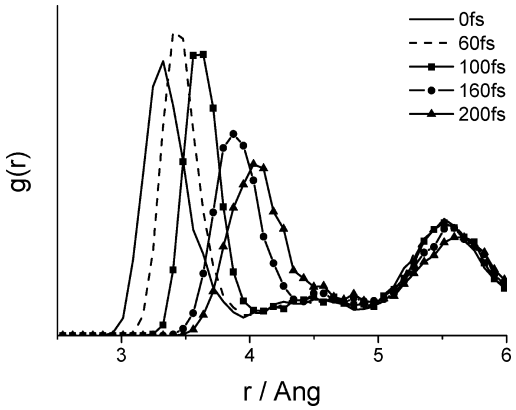

Figure 6. Time-dependent radial distribution functions of Ne around the NO impurity over 200 fs.

in this study are expected to be valid only up to ~1 ps, over which the simulated dynamical response does not depend on the simulation cell size. Such a limitation of MD simulations has been already discussed.[38,39] As previously suggested,[37,38] the quantum nature of the environment plays a significant role exclusively through the delocalization of the atoms in the lattice, whereas the exact nature of the interatomic correlations assumes a critical importance at later times. Within 1 ps, the MD simulations performed using the adjusted BM and Morse potentials for the NO(A)−Ne are in reasonable agreement with experiment. A closer look at the time evolution of the radial distribution function on a short time scale (Figure 6) reveals a nearly adiabatic expansion of the first shell (12 atoms) during <200 fs after excitation. This suggests that the three first shells around the chromophore are not set in motion impulsively during the first 200 fs. As previously proposed,[43] this effect is observed for longer times. This is the direct consequence of the shorter range of the adjusted BM and Morse NO(A)−Ne potential used here. Nevertheless, after 200 fs, this shell completely merges into the second one. Consequently, the expansion slows down up to ~600 fs, where the contraction begins. The two time scales for the electronic bubble expansion are similar to the ones evidenced experimentally and theoretically for solid hydrogen.[37−39] The spatial delocalization of the Ne atoms associated with the weakness of the Ne−Ne interaction lead to a drastic change of the local shell structure upon Rydberg excitation. The relative slow time scale for bubble expansion in Neon with respect to Argon is thus presumably related to the merging of the first two shells surrounding NO. This feature stems from the local disorder due to the quantum character of the lattice. For solid neon, the two time scales for expansion could not be experimentally evidenced because of the pump/probe cross correlation time (~320 fs), limiting the time resolution and the lack of points within the 300 fs to 1 ps time window.[28] In the case of classical solids,[29,30,45,46] the shell structure is preserved, and coherent oscillations of the first shell are evidenced. Such ultrafast recurrences do not exist in solid hydrogen,[37−39] for which the major part of energy impulsively deposited flows irreversibly to the medium over the picosecond time scale. It has to be noticed, however, that a weak recurrence after 10 ps suggests that an extremely low fraction of the energy remains localized around the impurity.

In solid neon, the behavior is intermediate between the classical and quantum cases as the local shell structure is destroyed, whereas the picosecond time scale oscillations appear in both experiments and the MD simulation. The recurrence experimentally observed around 1.4 ps cannot be quantitatively

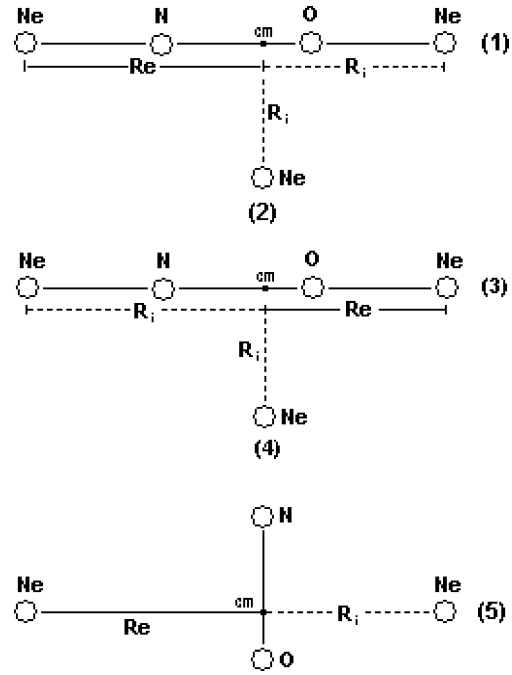

Figure 7. Schematic representation of five angular configurations studied to evaluate the contribution of three body interactions in the first Rydberg state.

reproduced theoretically because of the above-mentioned limitation of our MD simulation .

As shown in Figure 4a,b, the results obtained using the full ab initio PES for the NO−Ne interaction do not lead to a better description of the dynamical response than using the fitted two body pair potential. This might be related to the fact that all atoms of Ne around the NO impurity in the solid matrix modify the real interaction potential via many body effects. As a matter of fact, in our previous determination of the ab initio PES for the excited state, significant collision-induced dipole effects have been revealed.[50] This fact combined with the many-body nature of the matrix suggested to us that the pair additive assumption used to build the total interaction potential could be the source of the observed discrepancies. One could argue that the adjusted 1D potentials may include the many-body effects in an effective potential way, whereas the 2D ab initio potential does not include them at all. For this reason, we performed model calculations to determine the relevance of three-body effects in this system.

To evaluate the contribution of three body interaction in the first Rydberg state, the energy of the Ne−NO−Ne system was calculated using ab initio methodology.

In Figure 7, the five angular configurations studied are shown. In this calculation, we maintain constant the NO bond length, r, at its equilibrium value (1.06 Å), and the intermolecular distance of one Ne−NO complex, R_e, was maintained at the equilibrium value corresponding to each configuration (6.5 Å for cases 1−4 and 7.0 Å for case 5). The intermolecular energies, E_{3B}, are calculated for several distances of the other Ne atom from the center of mass of NO, R_i (3.0−8.0 Å in each case).

We use the same methodology as that in our previous calculation of the Ne−NO intermolecular potential.[50] In brief, this includes a high-level treatment of electron correlation with coupled cluster singles and doubles with perturbative correction for triple excitations (CCSD(T)) together with an extensive basis set composed of augmented valence triple zeta (AVTZ) for all

TABLE 2: Relative Three-Body Contribution for Five Angular Configurations

	difference (%)				
$R(i)$	case 1	case 2	case 3	case 4	case 5
3.00	0.03	0.02	0.02	0.05	0.06
3.50	0.08	0.03	0.42	0.04	0.04
4.00	0.06	0.05	0.91	0.05	0.06
4.50	0.20	0.01	0.09	0.26	0.15
5.00	0.73	0.24	**2.98**	0.66	0.21
5.50	1.35	0.31	0.88	**5.63**	1.82
6.00	**2.20**	0.00	2.30	4.84	0.58
6.50	0.91	0.00	0.88	2.63	0.16
7.00	1.07	0.49	0.78	3.67	**3.29**
8.00	0.96	**0.64**	0.00	1.67	1.59

atoms, extra sets of diffuse functions, and bond functions for an accurate representation of the van der Waals interactions. The interaction energies have been corrected for the basis set superposition error.

The three-body contribution is evaluated as

$$\mathrm{TB_c} = \left|\frac{E_{3B} - E_{2B}}{E_{3B}}\right| \times 100$$

where E_{2B} represents the two-body approximation to the total interaction potential obtained from equivalent calculations of the Ne−NO complex. A comparison is displayed in Table 2.

It is interesting to see that the three-body effects are relatively more important in the long range and become nearly irrelevant in the short range. On a short time scale, the energy released into the system (0.9 eV) is shared by very few atoms (about 18 up to 600 fs). This amount of energy is huge with respect to the small corrections because of many body interactions. From these results, it is clear that the neglect of higher many-body effects in the calculation of the interaction potential for NO in the Ne matrix is not responsible for the poor agreement between the MD results using the ab initio and empirically fitted potentials; therefore, this point deserves further comment. In a recent work,[58] it has been shown that by using the same ab initio methodology as that applied here it has been possible to predict the binding energies and van der Waals vibrational levels of the series NO(A)−Rg (Rg = Ne, Ar, Kr, Xe) in good agreement with experimental spectra. This is a very stringent test for the quality of the interaction potential. The matrix relaxation processes studied in the present work depend crucially on the slope of the potential in the repulsive region of the interaction. Further ab initio testing is necessary to decide if the methodology used loses reliability in that region.

4. Conclusions

The local relaxation dynamics of solid neon upon the Rydberg excitation of a NO chromophore has been studied via MD simulation including a thermal quantum correction to account for the zero-point energy quantum delocalization of the Ne atoms about the lattice sites. The influence of the NO−Ne interaction potential on the relaxation dynamics has been scrutinized. In particular, one of the main motivations for the present work was to use a more realistic description of the NO−Ne interaction because all previous studies had neglected the molecular properties of NO and used empirical atom−atom potentials. Our results show that the 2D ab initio representation of the NO−Ne interaction does not lead to a better description of the energy relaxation than the empirical pair potentials adjusted on steady-state spectroscopic data. The precise explanation for this discrepancy remains to be investigated. The relaxation dynamics on a 1 ps time scale is well predicted by our MD simulation. It was previously believed that the relative slow relaxation of solid neon with respect to argon was due to the longer range of the NO(A)−Ne interaction. In this article, we also suggest that the local disorder resulting from the quantum character of the medium might also play an important role. The response involves a local destruction of the shell structure as well as picosecond oscillations, which are, respectively, typical of quantum (e.g., H_2) and classical solids (e.g., Ar).

Acknowledgment. P.P.S. and R.H.L. would like to thank Conacyt for financial support through grant 44117F. G.R.L., P.P.S., and J.R.S. would like to thank the National Program of Basics Science for financial support through grant PNCB/2.

References and Notes

(1) Jortner J. In *Femtochemistry: Ultrafast Chemical and Physical Processes in Molecular Systems*; Chergui, M., Ed.; World Scientific: Singapore, 1996; p 15 and references therein.
(2) Benjamin, I.; Wilson, K. R. *J. Chem. Phys.* **1989**, *90*, 4176.
(3) Liu, Q. L.; Wan, C.; Zewail, A. H. *J. Phys. Chem.* **1996**, *100*, 18666.
(4) Krylov, I.; Gerber, R. B. *J. Chem. Phys.* **1994**, *100*, 4242.
(5) Batista, V. E.; Coker, D. F. *J. Chem. Phys.* **1996**, *105*, 4033.
(6) Laage, D.; Hynes, J. T. *Proc. Natl. Acad. Sci. U.S.A.* **2007**, *104*, 11167.
(7) Jungwirth, P.; Winter, B. *Annu. Rev. Phys. Chem.* **2008**, *59*, 343.
(8) Schwentner, N.; Apkarian, V. A. *Chem. Rev.* **1999**, *99*, 1481.
(9) (a) Alimi, R.; Gerber, R. B.; Apkarian, V. A. *J. Chem. Phys.* **1988**, *89*, 174. (b) Alimi, R.; Apkarian, V. A.; Gerber, R. B. *J. Chem. Phys.* **1993**, *98*, 331.
(10) Gerber, R. B.; Krylov, A. I. *Reaction Dynamics in Clusters and Condensed Phase*; Jortner, J., Levine, R. D., Pullman, B., Eds.; Kluwer Academic Publishers: Dordrecht, The Netherlands, 1994; p 509.
(11) (a) Zadoyan, R.; Li, Z.; Martens, C. C.; Apkarian, V. A. *J. Chem. Phys.* **1994**, *101*, 6648. (b) Li, Z.; Zadoyan, R.; Apkarian, V. A.; Martens, C. C. *J. Phys. Chem.* **1995**, *99*, 7435.
(12) (a) Gersonde, H.; Gabriel, H. *J. Chem. Phys.* **1993**, *98*, 2094. (b) Gersonde, I. H.; Hennig, S.; Gabriel, H. *J. Chem. Phys.* **1994**, *101*, 9558.
(13) Bargheer, M.; Cohen, A.; Gerber, R. B.; Guhr, M.; Korolkov, M. V.; Manz, J.; Niv, M. Y.; Schroder, M.; Schwentner, N. *J. Phys. Chem. A* **2007**, *111*, 9673.
(14) Guhr, M.; Bargheer, M.; Fushitani, M.; Kiljunen, T.; Schwentner, N. *Phys. Chem. Chem. Phys.* **2007**, *9*, 779.
(15) Kiljunen, T.; Bargheer, M.; Guhr, M.; Schwentner, N. *Phys. Chem. Chem. Phys.* **2004**, *6*, 2932.
(16) Kiljunen, T.; Bargheer, M.; Guhr, M.; Schwentner, N.; Schmidt, B. *Phys. Chem. Chem. Phys.* **2004**, *6*, 2185.
(17) Bargheer, M.; Schwentner, N. *Low Temp. Phys.* **2003**, *29*, 165.
(18) (a) Amar, F. G.; Berne, B. J. *J. Chem. Phys.* **1984**, *88*, 6720. (b) Perera, L.; Amar, F. G. *J. Chem. Phys.* **1989**, *90*, 7354.
(19) (a) Liu, Q.; Wang, J.-K.; Zewail, A. H. *Nature* **1993**, *364*, 427. (b) Wang, J.-K.; Liu, Q.; Zewail, A. H. *J. Phys. Chem.* **1995**, *99*, 11321.
(20) Nahler, N. H.; Fárník, M.; Buck, U.; Vach, H.; Gerber, R. B. *J. Chem. Phys.* **2004**, *121*, 1293.
(21) Schwentner, N.; Koch, E. E.; Jortner, J. *Electronic Excitation in Condensed Rare Gas Solids*; Springer: Berlin, 1985.
(22) Bondybey, V. E. *Adv. Chem. Phys.* **1980**, *41*, 269.
(23) Suemoto, T.; Kanzaki, H. *J. Phys. Soc. Jpn.* **1980**, *49*, 1039.
(24) Suemoto, T.; Kanzaki, H. *J. Phys. Soc. Jpn.* **1981**, *50*, 3664.
(25) Leung, C. H.; Emery, L.; Song, K. S. *Phys. Rev. B* **1984**, *28*, 3474.
(26) Inoue, K.; Sakamoto, H.; Kanzaki, H. *J. Phys. Soc. Jpn.* **1984**, *53*, 819.
(27) Coletti, F.; Debever, J. M.; Zimmerer, H. *J. Chem. Phys.* **1985**, *83*, 49.
(28) Vigliotti, F.; Bonacina, L.; Chergui, M. *Phys. Rev. B* **2003**, *67*, 115118.
(29) Jeannin, C.; Portela-Orbeli, M. T.; Jimenez, S.; Vigliotti, F.; Lang, B.; Chergui, M. *Chem. Phys. Lett.* **2000**, *316*, 51.
(30) Jimenez, S.; Pasquarello, A.; Car, R.; Chergui, M. *Chem. Phys.* **1998**, *233*, 343.
(31) Nisoli, M.; DeSilvestri, S.; Svelto, O.; Scholz, R.; Fanciulli, R.; Pellegrini, V.; Beltram, F.; Bassani, F. *Phys. Rev. Lett.* **1996**, *77*, 3463.
(32) Dhar, L.; Rogers, J. A.; Nelson, K. A. *Chem. Rev.* **1994**, *94*, 157.

(33) Tokizaki, T.; Akiyama, H.; Nakamura, A.; Tanimura, K.; Itoh, N. *Phys. Rev. Lett.* **1991**, *67*, 2701.
(34) Vigliotti, F.; Chergui, M.; Dickgiesser, M.; Schwentner, N. *Faraday Discus.* **1997**, *108*, 139.
(35) Vigliotti, F.; Cavina, A.; Bressler, Ch.; Lang, B.; Chergui, M. *J. Chem. Phys.* **2002**, *116*, 4542.
(36) Vigliotti, F.; Bonacina, L.; Chergui, M. *J. Chem. Phys.* **2002**, *116*, 4553.
(37) Bonacina, L.; Larrégaray, P.; van Mourik, F.; Chergui, M. *J. Chem. Phys.* **2006**, *125*, 054507.
(38) Bonacina, L.; Larrégaray, P.; van Mourik, F.; Chergui, M. *Phys. Rev. Lett.* **2005**, *95*, 015301.
(39) Egorov, S.; Larregaray, P. *J. Chem. Phys.* **2008**, *128*, 244502.
(40) Cui, S.; Johnson, R. E.; Cummings, P. T. *Phys. Rev. B* **1989**, *39*, 9580.
(41) Jimenez, S.; Chergui, M.; Rojas-Lorenzo, G.; Rubayo-Soneira, J. *J. Chem. Phys.* **2001**, *12*, 5264.
(42) Castro-Palacio, J. C.; Velazquez, L.; Rojas Lorenzo, G.; Rubayo-Soneira, J. *Eur. Phys. J. D* **2003**, *25*, 149–155.
(43) Rojas-Lorenzo, G.; Rubayo-Soneira, J.; Vigliotti, F.; Chergui, M. *Phys. Rev. B* **2003**, *67*, 115119.
(44) Rubayo-Soneira, J.; Castro-Palacio, J. C.; Rojas Lorenzo, G. *Phys. Stat. Solidi B* **2005**, *242*, 1747–1753.
(45) Castro-Palacio, J. C.; Rubayo-Soneira, J.; Ishii, K.; Yamashita, K. *J. Chem. Phys.* **2007**, *126*, 134315.
(46) Castro-Palacio, J. C.; Rubayo-Soneira, J.; Lombardi, A.; Aquilanti, V. *Int. J. Quantum Chem.* **2008**, *108*, 1821.
(47) Bergsma, J. P.; Berens, D. R.; Wilson, K. R.; Fredkin, D. R.; Heller, E. J. *J. Phys. Chem.* **1984**, *88*, 612.
(48) Thuis, H. H. W.; Stolte, S.; Reuss, J.; Van den Biessen, J. J. H.; Van den Meijdenberg, C. J. N. *Chem. Phys.* **1980**, *52*, 211.
(49) Vigliotti, F.; Chergui, M. *Chem. Phys. Lett.* **1998**, *296*, 316; **1999**, *296*, 187.
(50) Pajón-Suárez, P.; Rojas-Lorenzo, G.; Rubayo-Soneira, J.; Hernández-Lamoneda, R. *Chem. Phys. Lett.* **2006**, *421*, 389–394.
(51) García, A.; Rubayo-Soneira, J.; Delgado-Barrio, G.; Villarreal, P. *J. Chem. Phys.* **1996**, *104*, 8405.
(52) Aziz, R. A.; Slaman, M. J. *Chem. Phys.* **1989**, *130*, 187.
(53) Carrasquillo, E.; Langridge-Smith, P. R. R.; Levy, D. H. In *Laser Spectroscopy Y*; McKellar, A. R. W., Oka, T., Stoicheff, B. P., Eds.; Springer: Berlin, 1981; p 333.
(54) Vigliotti, F.; Bonacina, L.; Chergui, M.; Rojas-Lorenzo, G.; Rubayo-Soneira, J. *Chem. Phys. Lett.* **2005**, *362*, 31–38.
(55) Larrégaray, P.; Cavina, A.; Chergui, M. *Chem. Phys.* **2005**, *308*, 13–25.
(56) Allen, M.; Tildesley, T. *Computer Simulations of Liquids*; Clarendon: London, 1992.
(57) Uranga-Piña, L1.; Martínez-Mesa, A.; Rubayo-Soneira, J.; Rojas-Lorenzo, J. *Chem. Phys. Lett.* **2006**, *429*, 450.
(58) Klos, J.; Alexander, M. H.; Hernández-Lamoneda, R.; Wright, T. G. *J. Chem. Phys.* **2008**, *129*, 244303.
(59) Uranga-Piña, L. L.; Martínez-Mesa, A.; García-Reyes, L.; Rubayo-Soneira, J. *Phys. Chem. Chem. Phys.* **2009**, *11*, 5358.
(60) Kometer, R.; Legay, F.; Legay-Sommaire, N.; Schwentner, N. *J. Chem. Phys.* **1994**, *100*, 8737.
(61) Chergui, M.; Schwentner, N.; Chandrasekharan, V. *J. Chem. Phys.* **1988**, *89*, 1277.

JP903538F